MULTIPLE FLOW INTERACTIONS IN A PROPLYD BINARY SYSTEM
I. THE INTERPROPLYD SHELL

William J. Henney

Instituto de Astronomía, Universidad Nacional Autónoma de México, Campus Morelia, México

RESUMEN

El proplyd 168–326 (LV 1) en la nebulosa de Orión consta de un par de flujos fotoevaporativos, uno del disco circunestelar de cada miembro de un sistema binario protoestelar. Los dos flujos colisionan a velocidades ligeramente supersónicas, formando así una cáscara interproplyd densa acotada por dos choques débiles, mientras que otras interacciones ocurren entre los dos flujos fotoevaporativos individuales y el viento estelar de la estrella ionizante θ^1 Ori C. Muestro cómo las observaciones de la cáscara interproplyd permiten acotar adecuadamente la posible geometría del sistema binario, y además investigo hasta qué grado los choques débiles pueden contribuir directamente a la emisión observada de la cáscara en longitudes de onda visibles y de radio.

ABSTRACT

The Orion nebula proplyd 168–326 (LV 1) consists of a pair of photoevaporation flows, one from the circumstellar disk of each member of a protostellar binary system. The two flows collide at mildly supersonic velocities, producing a dense interproplyd shell bounded by two weak shocks, while further interactions occur between the individual photoevaporation flows and the stellar wind from the ionizing star θ^1 Ori C. I show how observations of the interproplyd shell allow the geometry of the binary system to be usefully constrained and investigate to what extent the weak shocks may directly contribute to the observed shell emission at optical and radio wavelengths.

Key Words: **H II REGIONS — HYDRODYNAMICS — BINARIES: VISUAL — STARS: PRE-MAIN SEQUENCE — STARS: MASS LOSS**

1. INTRODUCTION

The bright proplyds in the Orion nebula are the result of circumstellar accretion disks around young low- and intermediate-mass stars of the Trapezium stellar cluster being externally photoevaporated by the ultraviolet radiation from the O7V star θ^1 Ori C and other high-mass stars found at the center of the cluster (see O'Dell 2001 and references therein).

Many of the proplyds within a projected distance of $10''$ from θ^1 Ori C (corresponding to 6.45×10^{16} cm for an assumed distance of 430 pc) show evidence of interaction with the stellar wind from the ionizing star. This takes the form of faint arcs, visible in optical emission lines (Bally et al. 1998) and mid-infrared dust emission (Hayward, Houck, & Miles 1994), that lie $\sim 1''$ from the proplyds in the direction of θ^1 Ori C. These arcs have been successfully modelled (García-Arredondo, Henney, &

Arthur 2001) as a supersonic two-wind interaction between the fast stellar wind from the O star and the dense, transonic photoevaporation flow from the proplyd, as illustrated in Figure 1*a*. The shocked stellar wind gas is too hot ($\simeq 10^8$ K) and tenuous ($\simeq 1$ cm^{-3}) to be directly observable, whereas the shocked proplyd flow forms a dense ($\simeq 10^4$ cm^{-3}) shell, observable as an emission line/MIR arc.

The fraction of binary systems among low-mass stars in the Trapezium cluster has been shown to be similar to that of the field population (Bate, Clarke, & McCaughrean 1998; Petr et al. 1998) and is somewhat lower than that seen in lower-density star-forming environments such as Taurus-Auriga. The mean surface density of companions indicates a roughly uniform distribution of the logarithm of the binary separation in the range 25–500 AU and is consistent with $\sim 10\%$ of all systems being bina-

ries with separations in this range. The situation for larger separations is unclear since the high stellar density in the cluster means that chance superpositions of cluster stars dominate for separations > 500 AU. Nonetheless, analysis of proper motion data (Scally, Clarke, & McCaughrean 1999) suggests that there may be a real deficit of binaries with separations > 1000 AU, possibly the result of disruptions due to encounters with other stars.

For the closer-in proplyds, the relevant linear scales range from the accretion disk radii of < 50 AU up to the $\simeq 500$ AU size of the standoff arcs. Hence, proplyd binary systems with separations in this range should show interesting phenomena. For separations of order 100 AU, the individual accretion disks would be disrupted, whereas larger separations may lead to one proplyd shadowing the other or to hydrodynamic interactions between the two photoevaporation flows. A possible example of shadowing is the proplyd 159–350 (HST 3), in which a small binary companion (projected separation $\simeq 200$ AU) seems to cause an asymmetry in the appearance of the ionization front of the larger proplyd. Evidence for hydrodynamic interaction is seen most clearly between the proplyds 168–326 SE and NW, which comprise the LV 1 system (Graham et al. 2002), also with a projected binary separation of $\simeq 200$ AU, but lying much closer to the ionizing star θ^1 Ori C. Such an interaction is shown schematically in Figure 1b: an interproplyd shell forms where the two photoevaporation flows collide and the shocked gas in this shell must subsequently interact in some way with the fast stellar wind from θ^1 Ori C and with the standoff shells of the individual proplyds. In LV 1, a region of diffuse emission is seen between the two proplyds, which presumably corresponds to the interproplyd shell. In addition, the standoff arc shows a complex asymmetrical structure, attributable to its interaction with the interproplyd shell. In this paper we analyse in detail the properties of the interaction region between two proplyd outflows using semi-analytic techniques, with particular emphasis on the LV 1 system. A three-dimensional numerical hydrodynamical simulation of the interaction will be presented in a companion paper (Henney, García-Arredondo, & Arthur 2002), which will also consider the further interactions with the stellar wind from θ^1 Ori C.

2. INTERPROPLYD SHOCK IN LV 1

The LV 1 system consists of two proplyds, the larger being 168–326 SE and the smaller being 168–326 NW. The UV radiation from θ^1 Ori C drives a transonic photoevaporation flow from each proplyd and where these flows collide a dense shell bounded by two weak shocks will form. The interaction between two hypersonic, non-accelerating, spherical winds, forming an axisymmetric bowshock structure has been studied by Cantó, Raga, & Wilkin (1996, hereafter CRW) under the approximation that the interaction region forms a thin, momentum-conserving shell. The situation with the proplyds is rather more complicated, not least because the individual winds are non-isotropic and hence the resulting bowshock will be totally asymmetric. Nonetheless, the gross features of the interaction will be similar:

1. There will exist a point, termed the *stagnation point*, where the shell surface is perpendicular to the velocity vectors of both winds.[1] This forms the nose of the bowshock and its position is determined by the condition of ram pressure balance: it will be closer to the less powerful of the two proplyds in terms of wind momentum flux. The normal to the shell surface at the stagnation point can be considered the *axis* of the bowshock, even though it is not an axis of symmetry.

2. The shell will curve back toward the less powerful of the two winds. At each azimuth around the bowshock axis, the shell will tend asymptotically to a constant opening angle from the axis, but the anisotropy of the winds will lead to this opening angle varying with azimuth.

I discuss the peculiar 3-dimensional nature of the proplyd-proplyd interaction in § 3, and show how observed properties of the 168–326 system can be used to pin down the various angles involved. I then outline in § 4 how the 3-d problem can be usefully approximated as a 2-d problem, for which the formalism of CRW can be applied. In § 5, I concentrate on the 1-d structure of the shell at the stagnation point, showing that the cooling zones behind the shocks are very thin and should contribute very little to the optical/NUV emission as compared with the bulk of the shocked shell, except in high-ionization emission lines. Finally, § 6 summarizes the results of the current analysis and its bearing on the interpretation of available observational data.

3. GEOMETRY

The geometry of the interaction between the two proplyd flows is illustrated in Figure 2. The z-axis is taken to be the symmetry axis of the larger proplyd, which is in the direction of the ionizing star θ^1 Ori C.

---

[1]But note that if the photoevaporation flows are not strictly radial, then there may be multiple stagnation points.
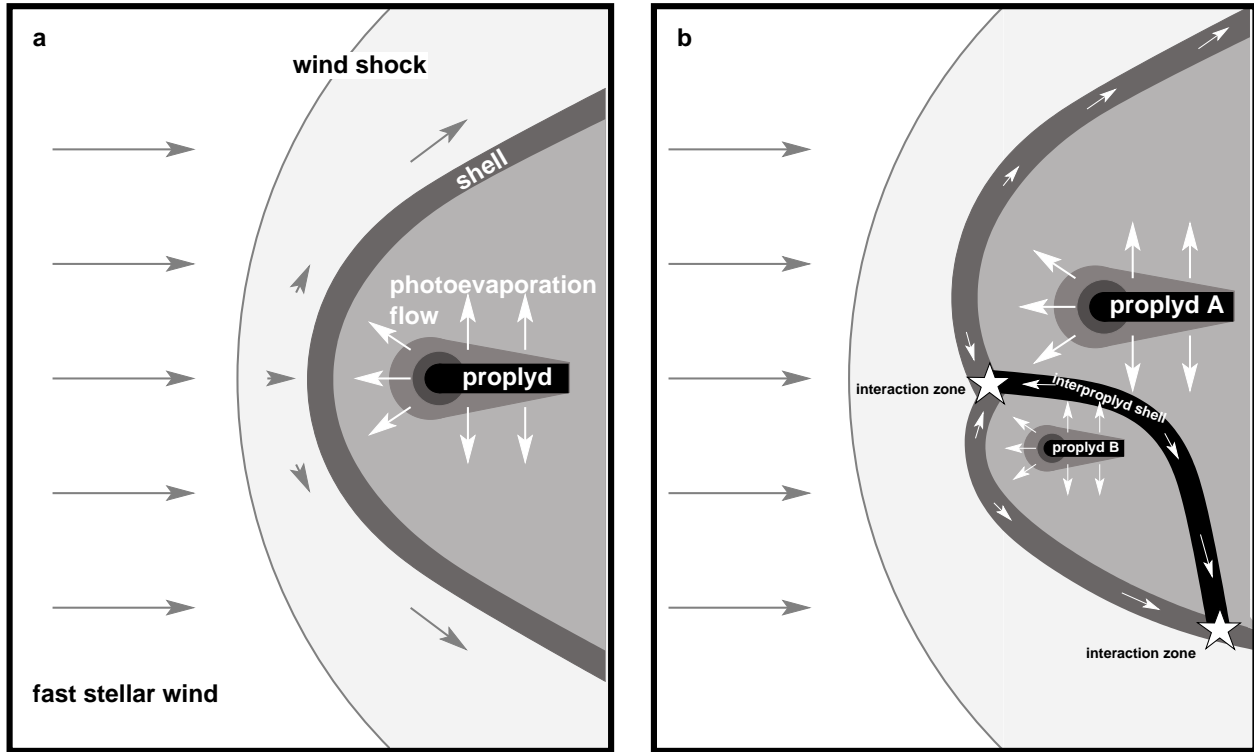
Fig. 1. (*a*) The two-wind interaction between the photoevaporation flow and the fast, tenuous stellar wind from the ionizing star. (*b*) The three-wind interaction that occurs in the case of binary proplyds. In addition to the standoff shell between each proplyd and the stellar wind, there is also an interproplyd shell. Furthermore, the gas in this interproplyd shell will subsequently interact with the standoff shells and the stellar wind at the regions indicated by stars in the figure.
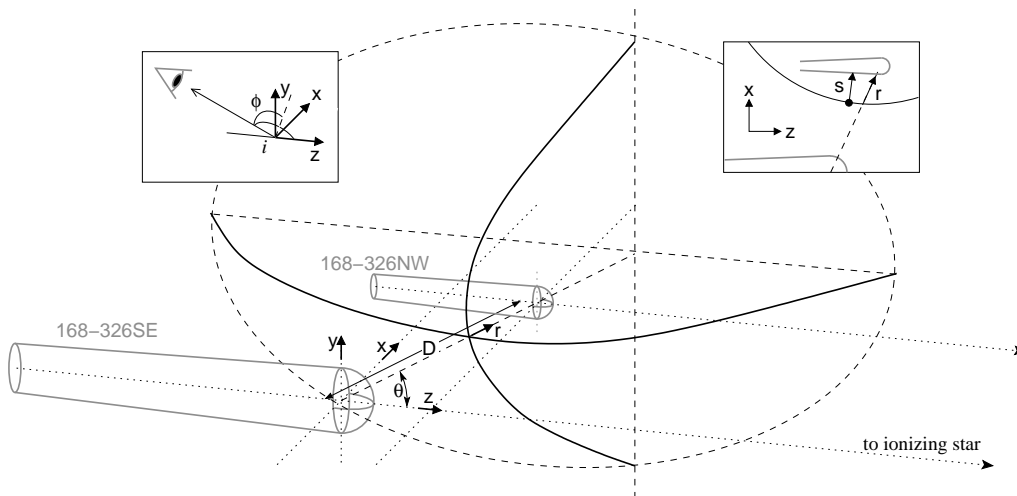
Fig. 2. Geometry of the proplyd-proplyd interaction zone. Left inset shows viewing orientation. Right inset shows how in general the stagnation point (black dot) need not lie on the line of centers and the normal, s, to the shock surface there need not be parallel to r.
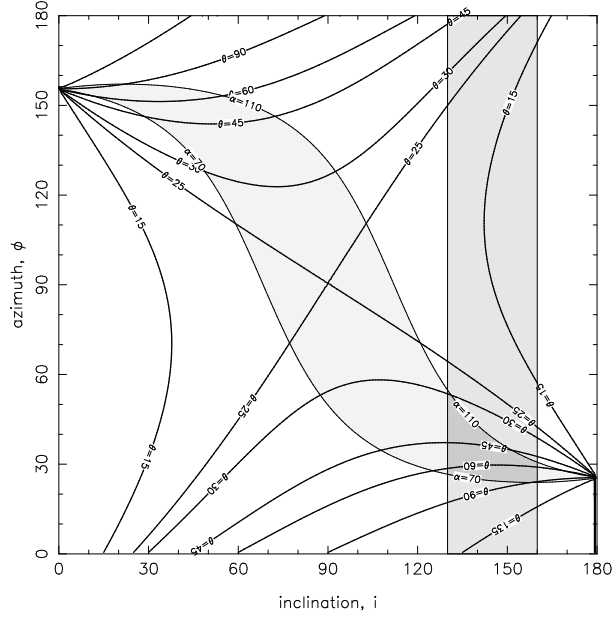
Fig. 3. Observational constraints on angular parameters of the LV 1 proplyd binary system. Heavy solid lines show contours in the inclination-azimuth plane of the angle θ between the binary separation and the proplyd axes (see Fig. 2), given that its observed value projected in the plane of the sky is $\theta' = 25°$. Light shading indicates the region allowed by the shell foreshortening constraint. Medium shading indicates the region allowed by inclination constraints. Dark shading indicates the overlap of the two regions.

Since the separation, D, of the two proplyds is small compared with the distance to θ^1 Ori C, I approximate the two proplyd axes as being parallel. The line joining the "flow center" of each proplyd[2] defines an axis r, which makes an angle θ with the z-axis and lies in the xz-plane. The normal to the "nose" of the bowshock defines a further axis, s, which in the case of two spherical winds would be identical to r, but in this asymmetric case need not be (see right inset of figure). The observer's line of sight (left inset of figure) makes an angle i with the z-axis and lies in a plane at an azimuthal angle of ϕ from the xz-plane. It is convenient to also introduce the angle α (not illustrated) that the line of sight makes with the s-axis.

In order to make progress with modeling the system, it is important to determine as well as possible the angles θ, α, i, and ϕ. To do this, one can make use of the several observational constraints as outlined below.

Constraint 1: Projected Value of θ   The *projected* angle θ' between the r and z can be measured to be $\simeq 25°$. From this, the true angle, θ, can be determined as

$$\tan\theta = \frac{\sin i}{\sin\phi\cot\theta' + \cos i\cos\phi}. \qquad (1)$$

Selected contours of θ are shown in Figure 3 as a function of i and ϕ. Note that only $\phi \leq 180°$ is allowed, since $\phi > 180°$ gives $\theta' < 0$ (i.e., secondary counterclockwise of primary as seen from θ^1 Ori C), contrary to what is observed.

Constraint 2: Inclination to Line of Sight The inclination, i, can be constrained in two ways via comparison with the proplyd 167–317 (LV 2), whose inclination ($i = 50 \pm 10°$) has been well-determined (Henney et al. 2002). First, spectroscopy of the [O III] $\lambda5007$ Å line (Henney et al. 1997, Fig. 2a) shows that the bulk of the emission from the proplyd flows in 168–326 is redshifted by an average of 10–20 km s^{-1} with respect to 167–317. The simplest explanation for this is that $i > 90°$ in 168–326, leading to the flow from the proplyd heads being directed away from the observer (the flow is toward the observer in 167–317). Second, if the peak surface brightnesses are compared (Henney & Arthur 1998), then one comes to the conclusion that 168–326 SE should be $\simeq 20\%$ more distant from θ^1 Ori C than 167–317, although its projected position is actually $\simeq 20\%$ closer. These can be reconciled if $\sin i$ is correspondingly smaller in 168–326 SE than in 167–317, implying $i \simeq 150°$. I hence adopt a conservative range of $i = 130$–$160°$ for the inclination of the 168–326 system,[3] which is shown as a gray box in Figure 3.

Constraint 3: Foreshortening of the Shell   A noteworthy feature of the *HST* images of the 168–326 system is that the emission from the inter-proplyd interaction zone appears elongated in the direction perpendicular to the projected separation of the proplyds. It is likely that this elongation is a projection effect rather than reflecting a real elongation of the shock/shell since any such elongation would be expected to be along the axis of the proplyds. If one assumes that the contours of shell brightness in the region of the stagnation point are intrinsically circular, then the aspect ratio of the elongation is simply $\cos\alpha$.[4] The relationship between α, i, and ϕ

---

[2]Although the position of this center is rather ill-defined, for concreteness in the figure I place it at the center of each proplyd's head.

[3]In which the fact that the reduction in surface brightness due to internal dust extinction will be greater for larger values of i has also been taken into account.

[4]This assumes that $\sin\alpha$ is sufficiently small that the brightest observed part of the shell is that corresponding to
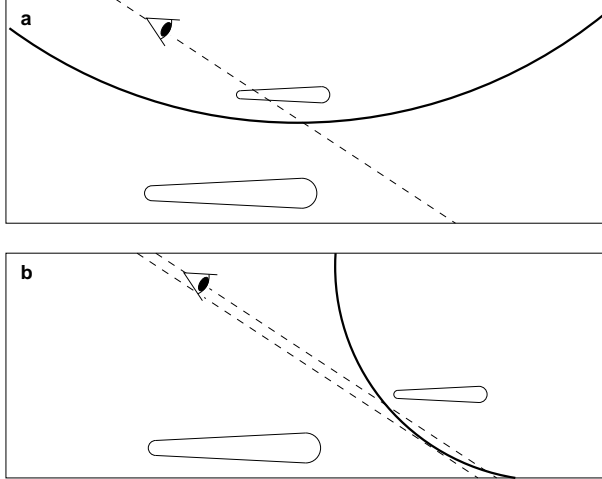
Fig. 4. Two possible geometrical configurations for the LV 1 binary sytem allowed by the 3 constraints of §3. (*a*) Side-by-side configuration: $\alpha < 90° \Rightarrow \theta \simeq 90°$ (*b*) Head-tail configuration: $\alpha > 90° \Rightarrow \theta \simeq 30°$. The observer's line of sight through the stagnation point of the shell is indicated by a dashed line (in reality the line of sight is slightly inclined with respect to the plane of the diagram). In (*b*) the lower dashed line indicates the line of sight that is tangent to the shell.

depends on whether or not the bowshock axis (*s*) is parallel to the proplyd separation (*r*). If it is, then the long axis of the projected elongation will automatically be perpendicular to the projection of *r*, as is in fact observed. In this case, one has that

$$\cos \alpha = \sin \theta \sin i \cos \phi + \cos \theta \cos i. \qquad (2)$$

The observed foreshortening is roughly a factor of 3, although it could be greater than this if the shell around the stagnation point is intrinsically elongated along the *z*-axis. This implies a value of $\alpha = 70$ to $100°$, which is shown on the $i\phi$-plane in Figure 3, together with its overlap with the allowed range of *i*.

Inspection of Figure 3 show that the combination of constraints 2 and 3 allows the determination of the azimuth of the line of sight to be $\phi = 25$–$55°$. This means that it is the smaller proplyd that lies in front of the interaction shell (as seen from the Earth) and the larger proplyd that lies behind it. There remain two broad possibilities for the angle, θ, between the binary separation and the proplyd axis: in the first possibility $\alpha < 90°$, which implies that one sees the stagnation region of the interproplyd shell from the direction of the smaller proplyd. From constraint 1,

the stagnation point rather than a limb-brightened rim. This is probably the case here, since otherwise the interproplyd shell would be expected to appear much sharper than it does (see below).

this then implies a value of θ in the range 60–90°— in other words, the two proplyds lie roughly side-by-side as seen from the ionizing star and the interaction is between their flanks. The second possibility is that $\alpha > 90°$ and one is seeing the interproplyd shell from the direction of the larger proplyd. This would imply $\theta = 30$–$45°$ so that the larger proplyd is behind the smaller one as seen from the ionizing star, with the head flow of the larger proplyd interacting from behind with the tail flow of the smaller one. These two possible configurations are illustrated in Figure 4.

It is apparent from Figure 4*b* that there are two problems with the head-tail configuration ($\alpha > 90°$). First, the stagnation point of the interproplyd shell would be seen to lie in between the tip of the tail of the smaller proplyd and the head of the larger one, whereas this does not seem to be the case from the observations. Instead, the interproplyd shell is seen to lie in projection just behind the head of the smaller proplyd and to be superimposed on its tail, which is consistent with Figure 4*a*, but not 4*b*. Second, for $\alpha > 90°$ the line of sight lies outside the "bowshock cone" so that there will be a point on the shell that is tangential to the line of sight (lower dashed line in Fig. 4*b*). This would produce a sharp limb-brightened arc that is not seen in the observations (see discussion of constraint 3 above and further discussion in Graham et al. 2002). On the other hand, the fact that the position of maximum brightness of the shell is slightly displaced from the line connecting the two proplyd heads (Graham et al. 2002) argues that θ cannot be exactly 90°.

In Graham et al. (2002), Fig. 9, the techniques of § 4, below, are extended somewhat in order to produce simulated emission images of CRW-type bowshocks in which the β parameter (and hence asymptotic opening angle) is allowed to vary with azimuth. It is shown that in this case, the ridge of emission between the proplyds can have a curved aspect when seen from within the bowshock cone, something which does not occur for cylindrically symmetric bowshocks (Graham et al. 2002, Fig. 8). This lends further support to the deductions in this section concerning the value of α.

It is therefore likely that the true configuration of the LV 1 system is close to that depicted in Figure 4*a*. For definitiveness, I adopt canonical values of $\theta = 80°$, $i = 150°$, $\phi = 25°$ in the discussion that follows.

4. REDUCTION TO 2 DIMENSIONS

In order to make further progress with the analysis of the inter-proplyd shell it is prudent to consider
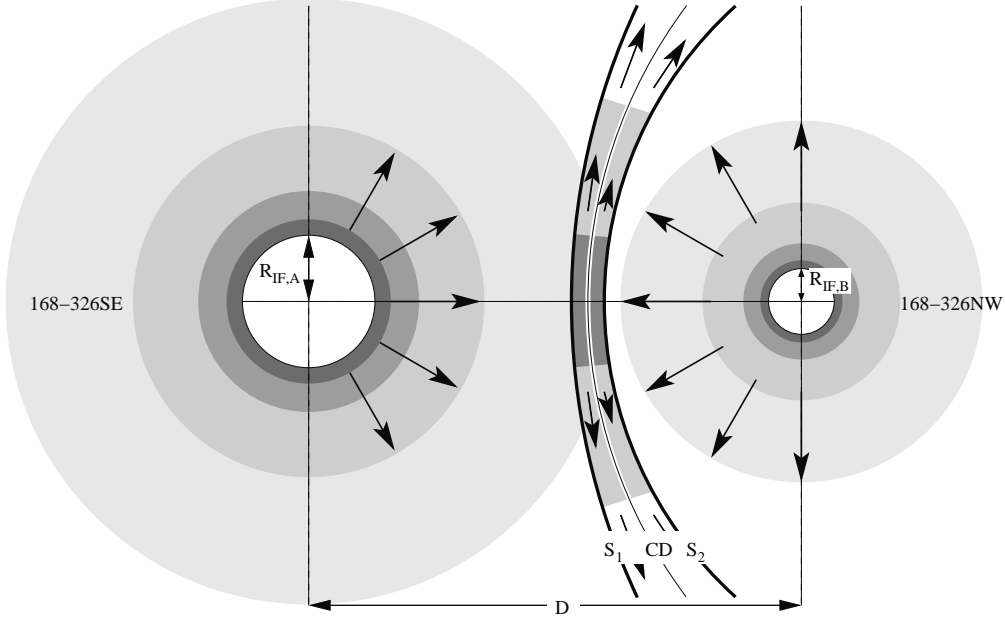
Fig. 5. Equivalent two-dimensional problem for the interaction of two proplyd outflows.

a reduced cylindrically-symmetric problem that can be treated in two dimensions rather than three. This will capture the most salient features of the interaction while greatly reducing the complexity of the calculation.

The reduced two-dimensional problem is illustrated in Figure 5: the proplyds are replaced by two spherical ionization fronts (IFs) separated by a distance D and having radii $R_{\mathrm{IF,A}}$, $R_{\mathrm{IF,B}}$ and densities at the IF $N_{\mathrm{IF,A}}$, $N_{\mathrm{IF,B}}$. The index A refers to the larger proplyd (168–326SE) and the index B to the smaller proplyd (168–326NW). The ionized outflow from each proplyd is assumed to be isothermal with an initial Mach number $\mathcal{M}$ of unity at R_{IF} and an acceleration law that can be approximated by a power law over the radial range of interest: $\mathcal{M}(x) = Ax^a$, where $x \equiv R/R_{\mathrm{IF}}$. The exact result for a spherical isothermal transonic flow (Dyson 1968) is reasonably well-fit on the range $x = 2$–4 (accuracy $< 2\%$) with $A = 1.91$, $a = 0.32$.[5]

In the real proplyd, the density at the IF is highest on the proplyd axis (N_0) since this receives direct perpendicular illumination from the ionizing star. The density declines around the cusp of the head and along the tail, as has been demonstrated by STIS observations of the NUV C III doublet ratio in the proplyd 167–317 (Henney et al. 2002, Fig. 11). Since the proplyd photoevaporation flow is

---

[5]Note, however, that this approximation fails badly outside its stated range of application.

"recombination-dominated" (see Henney 2001), the combination $N_0^2 R_{\mathrm{IF}}$ is directly proportional to the incident ionizing flux and is hence the same for both proplyds. In general, the relation between the peak density N_0 and the appropriate equivalent spherical density N_{IF} will be different for the two proplyds since it depends on their relative positions. However, in the case of the side-by-side configuration ($\theta = 90°$) discussed above then N_{IF}/N_0 will be approximately equal for the two proplyds. Hence, in this special case (which was shown in § 3 to be close to the likely configuration for the LV 1 system) one has

$$\frac{N_{\mathrm{IF,B}}}{N_{\mathrm{IF,A}}} \simeq \left(\frac{R_{\mathrm{IF,B}}}{R_{\mathrm{IF,A}}}\right)^{-1/2}. \qquad (3)$$

4.1. Location of the Stagnation Point

The interaction between the two flows will give rise to a shell bounded by two weak radiative shocks as shown in Figure 5. If the distance of the shell from the center of each proplyd is denoted by $R_{\mathrm{s,A}}$, $R_{\mathrm{s,B}}$, then ram pressure balance along the axis gives the following condition at the stagnation point

$$N_{\mathrm{IF,A}} \left(\frac{R_{\mathrm{s,A}}}{R_{\mathrm{IF,A}}}\right)^{a-2} = N_{\mathrm{IF,B}} \left(\frac{R_{\mathrm{s,B}}}{R_{\mathrm{IF,B}}}\right)^{a-2}. \qquad (4)$$

Combining this equation with equation (3) and using the fact that $R_{\mathrm{s,A}} + R_{\mathrm{s,B}} = D$, one finds the result

$$\frac{R_{\mathrm{s,A}}}{D} = \frac{1}{1 + \rho^n}, \quad \frac{R_{\mathrm{s,B}}}{D} = \frac{\rho^n}{1 + \rho^n}, \qquad (5)$$

where $\rho = R_{\mathrm{IF,B}}/R_{\mathrm{IF,A}}$ and $n = (3 - 2a)/(4 - 2a) \simeq 0.70$. Since $\rho < 1$ by definition and n is positive, one has that $R_{\mathrm{s,B}}/R_{\mathrm{s,A}} = \rho^n < 1$, implying that the stagnation point of the shell lies closer to the smaller proplyd. On the other hand, $x_{\mathrm{s,B}}/x_{\mathrm{s,A}} = \rho^{n-1} > 1$, so that the shell lies a *greater* number of IF radii from the smaller proplyd than from the larger one.

4.2. *Shape of the Shell*

The wings of the interaction shell will curve back toward the smaller proplyd, forming a shape that can be determined by considering momentum balance in a hypersonic thin shell (Wilkin 1996; CRW). Strictly speaking, two of the assumptions of the formalism presented by these authors are not satisfied in the present case: first, that the colliding winds are non-accelerating and, second, that, thermal pressure forces in the shell are negligible. However, since the acceleration of the wind is only gradual over the radial range of interest and given the drastic simplifications involved in the formulation of the 2-d problem, the CRW results should give a satisfactory approximation to the shape of the shell despite the violation of the first assumption. The second assumption does not affect the shape of the shell, but only the properties of the gas inside it, and is discussed further in the following section.

Comparison of equation (5) with CRW's equation (27) shows that CRW's β is equivalent to my ρ^{-2n}. The shell shape is then given by their equation (26) and, in particular, the asymptotic half-opening angle θ_∞ of the far wings of the bowshock shell is given by

$$\theta_\infty - \tan\theta_\infty = \frac{\pi}{1-\beta}. \qquad (6)$$

Alternatively, one can carry out a similar analysis to CRW but for two infinite aligned cylindical winds, rather than the spherical winds assumed by those authors. This may be a closer approximation to the interaction between the winds from the proplyd tails. In such a case, one finds

$$\theta_\infty = \cos^{-1}\left(\frac{\beta - 1}{\beta + 1}\right). \qquad (7)$$

The difference between the two cases is illustrated in Figure 6, where it can be seen that for cylindrical winds the wings of the interaction shell are slightly more swept-back for a given β than in the case of spherical winds.

4.3. *Density and Thickness of the Shell*

The analysis of CRW considers only the surface density of the shell and does not allow one to separately determine the volume density and thickness.
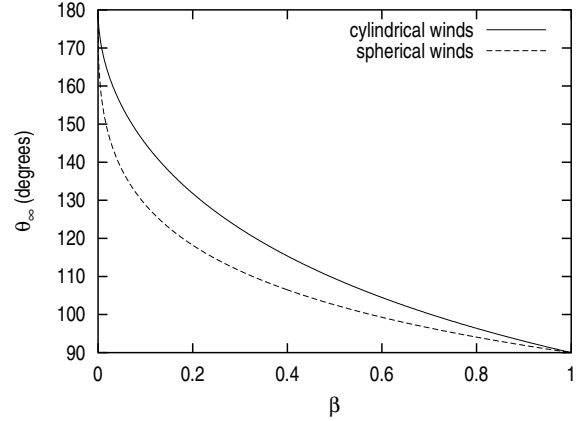
Fig. 6. Asymptotic opening angle, θ_∞, of the interaction shell as a function of the ratio of momentum-loss rates in the two winds, β. Results are shown for the cases of spherical winds (dashed line) and cylindrical winds (solid line). Only values of $\beta \leq 1$ are shown; results for $\beta > 1$ can be obtained by employing the transformation $\beta \rightarrow 1/\beta$, $\theta_\infty \rightarrow 180° - \theta_\infty$.

Nevertheless, these quantities are straightforward to calculate at the stagnation point. The density jumps by a factor of $\mathcal{M}^2$ across an isothermal shock, which means that the shell density on the axis is given by

$$N_{\mathrm{s}} = N_{\mathrm{IF,A}} x_{\mathrm{s,A}}^{-2} \mathcal{M}_{\mathrm{A}}, \qquad (8)$$

where $\mathcal{M}_{\mathrm{A}} = A x_{\mathrm{s,A}}^a$ is the proplyd flow Mach number just before the shock. Note that by equation (4) the same equation holds with A replaced by B throughout. By carrying out a small-angle expansion, equation (30) of CRW can be used to determine the surface density at the stagnation point. Combining this with equation (8) and converting all quantities to my notation gives the shell thickness[6] at the stagnation point as

$$h_0 = \frac{3}{4} D \left(\frac{1}{\mathcal{M}_{\mathrm{A}}} + \frac{1}{\mathcal{M}_{\mathrm{B}}}\right)^2 \left(\frac{R_{\mathrm{s,A}} R_{\mathrm{s,B}}}{D^2}\right). \qquad (9)$$

However, as mentioned above, the CRW calculation assumes hypersonic flow velocities everywhere, whereas in the proplyd case the flow will be subsonic in a significant portion of the shell, which reduces the value of the shell thickness somewhat from that given in equation (9). This is because pressure gradients assist the acceleration of the gas along the shell, hence reducing the surface density with respect to the hypersonic case. A solution in the general

---

[6]Following CRW, this result assumes full mixing across the contact discontinuity of the shell. If there is no mixing, then the result is slightly different, but only significantly so if $\mathcal{M}_{\mathrm{B}}$ differs greatly from $\mathcal{M}_{\mathrm{A}}$, which is not the case here.

case is difficult, but in the simpler case where $\rho = 1$ and $\mathcal{M}_A = \mathcal{M}_B$ then by considering mass and momentum conservation in the shell, including thermal pressure terms, one finds that the thickness of equation (9) must be multiplied by a correction factor

$$2 \left[1 + \left(1 + 18/\mathcal{M}_A^2 \right)^{1/2} \right]^{-1} .$$

It is shown below that $\mathcal{M}_A \simeq \mathcal{M}_B \sim 3$ for the LV 1 system, giving a correction factor of $\simeq 0.7$, which is not far enough from unity to justify a more elaborate calculation.

4.4. *Application to 168–326 and Comparison with Observations*

For the larger proplyd (168–326SE), the ionization front radius has been found to be $R_{IF,A} = 6.3 \pm 0.6 \times 10^{14}$ cm (Henney & Arthur 1998) by model-fitting to the Hα brightness distribution of the head. For 168–326NW application of this technique is more problematic since its head is barely resolved with the *HST*, but one finds $R_{IF,B} \sim 3 \times 10^{14}$ cm, which implies a ratio: $\rho \simeq 0.5$. This is consistent with the fact that the length of the tail of the smaller proplyd (as seen on the *HST* N II image) is roughly half that of the larger proplyd. The projected distance between the centers of the heads of the two proplyds can be measured to be $0.42''$, or $D' = 2.71 \times 10^{15}$ cm. This is related to the true separation D by $D' = D \sin \alpha$, where α is the angle between the line of sight and the s-axis given by equation (2). From constraint 3 of § 3, it was found that $\cos \alpha \simeq 0.3$ so that $D \simeq 1.05 D' \simeq 2.84 \times 10^{15}$ cm.

The peak ionized density of 168–326SE has also been determined as $N_0 = 2.33 \pm 0.04 \times 10^6$ cm^{-3} (Henney & Arthur 1998; García-Arredondo et al. 2001) but due to the side-by-side configuration the appropriate value for $N_{IF,A}$ will be somewhat less, as discussed at the start of this section. For 167–317 (Henney et al. 2002), the IF density at the head/tail boundary was found to be roughly $0.2 N_0$ and I will use the same value here, giving $N_{IF,A} \simeq 4.6 \times 10^5$ cm^{-3} and hence from equation (3) $N_{IF,B} \simeq 3.3 \times 10^5$ cm^{-3}.

From equations (5)–(9) one can then derive the following parameters for the interaction shell:

$$\frac{R_{s,A}}{D} = 0.62, \quad \frac{R_{s,B}}{D} = 0.38, \tag{10}$$

$$x_{s,A} = 2.8, \quad x_{s,B} = 3.4, \tag{11}$$

$$\mathcal{M}_A = 2.7, \quad \mathcal{M}_B = 2.8, \tag{12}$$

$$N_s = 0.34 N_{IF,A} = 1.6 \times 10^5 \text{ cm}^{-3}, \tag{13}$$

$$h_0 = 0.065 D = 1.8 \times 10^{14} \text{ cm}, \tag{14}$$

$$\beta = 2.64, \quad \theta_\infty = 63\text{–}73°. \tag{15}$$

From the *HST* and MERLIN images (Graham et al. 2002) one can measure $R_{s,A}/D = 0.65 \pm 0.05$, in good agreement with equation (10). Equation (14) predicts a shell thickness corresponding to an angular size of $\simeq 0.03''$, which is not resolvable with current instruments. This supports the argument in § 3 that the fuzzy appearance of the shell is due to it not being seen tangentially (see also Graham et al. 2002).

From equation (15) the bowshock shape of the shell is predicted to be very blunt and with rather wide-angle wings. This is supported by the general appearance of the shell, which is very flat and with a roughly uniform brightness that in the nose region falls off only slowly away from the axis.

Combining equations (13) and (14), one can calculate the perpendicular emission measure of the shell to be

$$N_s^2 h_0 = 4.52 \times 10^{24} \text{ cm}^{-5}, \tag{16}$$

which, assuming a pure recombination spectrum from gas at 10^4 K, implies a shell Hα surface brightness of

$$S_{H\alpha} = \frac{4.39 \times 10^{10}}{\cos \alpha} \text{ phots cm}^{-2} \text{ s}^{-1} \text{ sr}^{-1}. \tag{17}$$

The observed surface brightness of the shell (after correcting for foreground dust extinction with $\tau_{dust} = 1.16$, O'Dell & Yusef-Zadeh 2000) is $S_{H\alpha} = 7.6 \times 10^{11}$ phots cm^{-2} s^{-1} sr^{-1}. Hence, a value as low as $\cos \alpha \simeq 0.05$ is required if the recombination spectrum from the shell is to account for all the observed brightness. This is significantly lower than was suggested in § 3, but could be consistent with the observational constraints if the stagnation region were intrinsically elongated along the direction of the proplyd tails. Alternatively, emission from the shocks that bound the shell could enhance the emission. This is considered in the following section.

5. SHOCK EMISSION VS. SHELL EMISSION

In the previous section, it was assumed that the physical state of the gas in the interproplyd shell was just the photoionization equilibrium state at $\simeq 10^4$ K that obtains elsewhere in the nebula. However, immediately behind each of the two shocks that bound the shell, the gas temperature will be raised due to the thermalization of the pre-shock kinetic energy, which will result in enhanced emission as this excess

thermal energy is radiated away and the gas returns to its equilibrium state (see Figure 7).

The bolometric radiative flux of this "shock emission" will be equal to the kinetic energy flux $0.5\rho v^3$ through the shock. Adding the contributions from the two sides gives

$$F_{\text{shock}} = 0.5mc_0^3 N_{\text{IF,A}} x_{\text{s,A}}^{-2} \mathcal{M}_{\text{A}} \left(\mathcal{M}_{\text{A}} + \mathcal{M}_{\text{B}} \right), \quad (18)$$

where $m \simeq 1.3m_{\text{H}}$ is the mean mass per nucleon and $c_0 \simeq 12$ km s^{-1} is the photoionized sound speed. Inserting appropriate values from the previous section then gives $F_{\text{shock}} = 1.63$ erg cm^{-2} s^{-1} for the LV 1 system.

For comparison, the bolometric luminosity from the shell is given by

$$F_{\text{shell}} = N_{\text{s}}^2 h_0 \Lambda_{\text{s}}, \quad (19)$$

where Λ_{s} is the cooling coefficient (erg cm^3 s^{-1}) of the equilibrium gas. To evaluate Λ_{s} for the LV 1 shell, I used the photoionization code Cloudy (Ferland 2000) to calculate a model for an optically thin shell of the appropriate density located at the appropriate distance from θ^1 Ori C. The Cloudy model predicts that the shell electron temperature is $T_{\text{e}} = 9760$ K, that 99.9% of He is He$^+$, and that $\simeq 99\%$ C, N, and O are in the doubly-ionized state. The predicted cooling coefficient is $\Lambda_{\text{s}} = 3.3 \times 10^{-24}$ erg cm^3 s^{-1}, with major coolants being the optical [O III] 5007,4959 Å lines (46% of total) and H bound-free continuum (15%). Inserting this value in equation (19) together with the value for the emission measure from equation (16) gives $F_{\text{shell}} = 14.92$ erg cm^{-2} s^{-1}, which is nearly an order of magnitude higher than F_{shock}.

It is straightforward to show that, apart from geometrical factors, the principal functional dependencies of F_{shell} and F_{shock} are

$$F_{\text{shell}} \propto F_* \left(D/R_{\text{IF}} \right)^{-3}, \quad (20)$$

$$F_{\text{shock}} \propto F_* U_{\text{ion}}^{-1} \left(D/R_{\text{IF}} \right)^{2a-2}, \quad (21)$$

where F_* is the ionizing flux from the exciting star and U_{ion} is the ionization parameter: $U_{\text{ion}} = F_*/(cN_{\text{IF}})$. At larger distances from the IF, the velocity law of the proplyd flow becomes flatter and $a = 0.0$–0.3 is appropriate, giving the ratio of the two fluxes as

$$\frac{F_{\text{shock}}}{F_{\text{shell}}} \sim \frac{1}{U_{\text{ion}}} \left(\frac{D}{R_{\text{IF}}} \right)^{\delta}, \quad (22)$$

where $\delta = 1.0$–1.6. Hence, for proplyds of a given size the shock emission becomes relatively more important for larger binary separations D and also for

larger distances d_* from θ^1 Ori C (since $U_{\text{ion}} \propto d_*^{-1}$ if R_{IF} is fixed). For both of these cases, however, the absolute value of F_{shock} is actually reduced rather than increased, as can be seen from equation (21) since $a < 1$ and $F_* \propto d_*^{-2}$.

Although I have shown that the bolometric emission from the equilibrium shell dominates that from the shocks, the shock spectrum will be different from that of the shell and hence the shocks could make an important contribution to the strengths of some emission lines. In order to quantify this, it is necessary to consider the shock structure in more detail. Shocks in fully photoionized regions have a somewhat simpler structure than shocks in neutral gas and so published shock models cannot be used unchanged. The emission from a classical shock can be conceptually divided into 4 zones (Cox & Raymond 1985; Draine & McKee 1993): a pre-shock radiative precursor, an immediately post-shock ionization zone, a cooling zone, and a recombination zone.[7] For weak photoionized shocks, however, only the cooling zone is important: there is no precursor to speak of because the radiation from the shock is negligible compared to the ambient radiation. Also, collisional ionization rates in the post-shock gas are in the main unimportant compared with the photoionization rates, so the ionization and recombination zones are also absent.

The general structure of the flow variables along the symmetry axis of the bowshock shell is illustrated schematically in Figure 7. The approximately isothermal proplyd flow accelerates from the sound speed up to a Mach number $\mathcal{M}_0$ at the position of the shock. If the number density and temperature immediately before the shock are N_0, T_0, then the Rankine-Hugoniot conditions give the values immediately after the shock to be (Landau & Lifschitz 1982)

$$\mathcal{M}_1 = \left(\frac{\mathcal{M}_0^2 + 3}{5\mathcal{M}_0^2 - 1} \right)^{1/2}, \quad (23)$$

$$N_1 = \frac{4}{1 + 3\mathcal{M}_0^{-2}} N_0, \quad (24)$$

$$T_1 = \frac{1}{16} \left(5\mathcal{M}_0^2 - 1 \right) \left(1 + 3\mathcal{M}_0^{-2} \right) T_0. \quad (25)$$

For instance, using $\mathcal{M}_0 = \mathcal{M}_{\text{A}} = 2.7$ from equation (12), one obtains $\mathcal{M}_1 = 0.54$, $N_1 = 2.83N_0 = 5.77 \times 10^4$ cm^{-3}, $T_1 = 3.13T_0 = 30,500$ K, so that the density and temperature jump across the shock are both roughly a factor of 3.

The emission from the cooling zone behind the shock can be crudely approximated as the emission

---

[7]The last three may overlap to some extent.
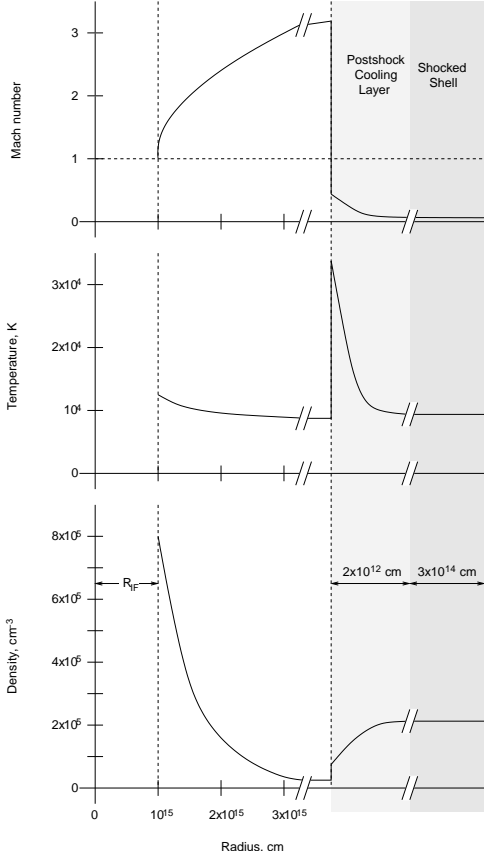
Fig. 7. One-dimensional structure of the interaction zone. The transonic flow accelerates away from the proplyd IF (unshaded region), passes through a shock after which it cools (light shaded region) until it has returned to the photoionization equilibrium temperature (dark shaded region).

from a homogeneous layer with density N_1 and temperature T_1 and with a width equal to the cooling time $t_{cool} = 3kT_1/(N_1\Lambda_1)$ multiplied by the immediate post-shock velocity $v_1 = \mathcal{M}_1(T_1/T_0)^{1/2}c_0 \simeq 11.5$ km s^{-1}. In order to estimate the cooling coefficient Λ_1 in the cooling zone I calculated another Cloudy model, identical to that mentioned above except that the electron temperature was artificially maintained at $T_e = T_1$. The result was $\Lambda_1 = 4.46 \times 10^{-23}$ erg cm^3 s^{-1}, giving a cooling time $t_{cool} = 4.9 \times 10^6$ s and a cooling zone thickness $h_{cool} = 5.64 \times 10^{12}$ cm. Although the O III optical lines are still significant coolants in the cooling zone (20% of total), they are now supplanted in importance by the C III NUV (28%) and FUV (26%) lines.

Table 1 shows the predicted perpendicular surface brightnesses for various observationally important emission lines and 5 GHz radio continuum for the equilibrium shell model and the sum of the two

TABLE 1

PREDICTED SURFACE BRIGHTNESSES[a]

	Shell	Shocks
Hα	3.13	0.023
[N II] 6584 Å	9.8×10^{-3}	2.7×10^{-4}
[O III] 5007 Å	6.82	0.56
[C III] 1909 Å	0.24	0.23
5 GHz free-free[b]	4.7×10^{-5}	2.8×10^{-7}

[a]Units: 10^{10} photons cm^{-2} s^{-1} sr^{-1}.

[b]Units of νF_ν (cgs).

shocks. Only for the C III lines do the shocks make a significant contribution. For O III the shock contribution is about 10%, roughly the same as for the bolometric luminosity (as would be expected since O III is a major coolant). For Hα and radio free-free continuum, the shocks contribute less than 1% of the emission. This is due to the fall in the emissivity of both these processes with increasing temperature, which suppresses the emission in the hotter post-shock cooling zone. The N II emission is virtually non-existent from either shock or shell, a direct result of the extremely low abundance of N$^+$ in the models.

6. SUMMARY AND DISCUSSION

In the previous sections I have first shown how a combination of observational constraints, together with a minimal set of assumptions, can allow one to tie down the complicated 3-d geometry of the LV 1 interacting proplyd binary system. Second, I have shown how, using these results and a slight generalization of the CRW momentum-conserving bowshock formalism, one can construct a 2-d approximation that allows one to calculate such properties as the density, thickness, and asymptotic opening angle of the interproplyd shell. Third, I have constructed 1-d shock models of the stagnation zone of the bowshock and investigated the relative contributions of the post-shock cooling zone and the equilibrium shell to the emission by various observationally interesting processes. The general scheme of the paper has been to start with the full geometrical complexity of the problem but with little physics, then to gradually add more physics while simultaneously simplifying the geometry.

Although in general the results of the present modeling are in agreement with the observations, there are two areas where puzzling discrepancies arise. First, the 5 GHz radio emission from the inter-

proplyd shell was found by Graham et al. (2002) to be much brighter than that predicted from thermal free-free emission at 10^4 K, given the observed Hα emission. There, it was argued that the observations could be explained if all the Hα and radio emission from the shell were to come from gas that was substantially hotter ($> 20,000$ K) than the photoionized equilibrium value. However, in this paper ($\S$ 5) it is shown that the high-temperature zone behind the shock is very thin and contributes essentially nothing to either the Hα or 5 GHz emission from the interaction zone.

The second discrepancy concerns the optical [N II] 6584 Å emission from the interaction zone, which was shown in $\S$ 5 to be almost non-existent. This is because the column density of the shell is so low as to make it optically thin to He Lyman continuum photons, with the result that Nitrogen is predominantly ionized to N^{++}. Nonetheless, *HST* PC images of LV 1 (Bally et al. 1998) clearly show that the interproplyd shell is visible in the f658n filter, albeit fainter with respect to the proplyd cusps than for Hα or [O III]. One possible explanation would be that the inter-proplyd shell were so closely aligned with the proplyd axes that the ionizing radiation only struck it glancingly, allowing a significant N^+ population to be present. It will be possible to test this hypothesis by means of hydrodynamic simulations (see below). Alternatively, the f658n filter may be passing significant amounts of Hα or continuum emission, although the published filter calibration constants (O'Dell & Doi 1999) would argue against this.

In order to test some of the simplifying assumptions that were necessary in the current paper, we are carrying out 3-dimensional hydrodynamic simulations of the LV 1 binary system (Henney et al. 2002). In addition, these simulations include the fast wind from θ^1 Ori C and will allow us to investigate the external interaction regions marked by stars in Figure 1*b*, which were impossible to incorporate into the current analytic framework. Comparison with the shape of the deformed standoff bowshock seen in this system will provide independent constraints on the geometry to those discussed in $\S$ 3.

REFERENCES

Bally, J., Sutherland, R. S., Devine, D., & Johnstone, D. 1998, AJ, 116, 293

Bate, M. R., Clarke, C., & McCaughrean, M. J. 1998, MNRAS, 297, 1163

Cantó, J., Raga, A. C., & Wilkin, F. P. 1996, ApJ, 469, 729 (CRW)

Cox, D. P. & Raymond, J. C. 1985, ApJ, 298, 651

Draine, B. T. & McKee, C. F. 1993, ARA&A, 31, 373

Dyson, J. E. 1968, ApSS, 1, 388

Ferland, G. J. 2000, in RevMexAASC, 9, Astrophysical Plasmas: Codes, Models, and Observations, eds. S. J. Arthur, N. Brickhouse, & J. Franco (Mexico City: Inst. Astron., UNAM), 153

García-Arredondo, F., Henney, W. J., & Arthur, S. J. 2001, ApJ, 561, 830

Graham, M. F., Meaburn, J., Garrington, S. T., O'Brien, T. J., Henney, W. J., & O'Dell, C. R. 2002, ApJ, in press

Hayward, T. L., Houck, J. R., & Miles, J. W. 1994, ApJ, 433, 157

Henney, W. J. 2001, in RevMexAASC, 10, The Seventh Texas-Mexico Conference on Astrophysics: Flows, Blows and Glows, eds. W. H. Lee & S. Torres-Peimbert (Mexico City: Inst. Astron., UNAM), 57

Henney, W. J., & Arthur, S. J. 1998, AJ, 116, 322

Henney, W. J., García-Arredondo, F., & Arthur, S. J. 2002, in preparation

Henney, W. J., Meaburn, J., Raga, A. C., & Massey, R. 1997, A&A, 324, 656

Henney, W. J., O'Dell, C. R., Meaburn, J., & Garrington, S. T. 2002, ApJ, 566, 315

Landau, L. D., & Lifschitz, E. M. 1982, Fluid Mechanics, 2nd ed. (Oxford: Pergamon Press)

O'Dell, C. R. 2001, ARA&A, 39, 99

O'Dell, C. R., & Doi, T. 1999, PASP, 111, 1316

O'Dell, C. R., & Yusef-Zadeh, F. 2000, AJ, 120, 382

Petr, M. G., Coudeé de Foresto, V., Beckwith, S. V. W., Richichi, A., & McCaughrean, M. J. 1998, ApJ, 500, 825

Scally, A., Clarke, C., & McCaughrean, M. J. 1999, MNRAS, 306, 253

Wilkin, F. P. 1996, ApJ, 459, L31

William J. Henney: Instituto de Astronomía, UNAM, Campus Morelia, Apartado Postal 3-72, 58090 Morelia, Michoacán, México (w.henney@astrosmo.unam.mx).